Local buckling behavior of hybrid steel I-sections under uniform bending: moment-rotation characteristic

Shuxian Chen, A.M.ASCE[1]; Jun-Zhi Liu, A.M.ASCE[2]; and Tak-Ming Chan, M.ASCE[3]

[1]Postdoctoral Fellow, Department of Civil and Environmental Engineering, Hong Kong Polytechnic University, Yuk Choi Road, Hong Kong 999077, China. Email: shu-xian.chen@connect.polyu.hk

[2]Associate Professor, School of National Safety and Emergency Management, Beijing Normal University, Zhuhai 519087, China. Email: jun-zhi.liu@bnu.edu.cn

[3]Professor of Structural Engineering, Department of Civil and Environmental Engineering, Hong Kong Polytechnic University, Yuk Choi Road, Hong Kong 999077, China. (Corresponding author). Email: tak-ming.chan@polyu.edu.hk

Abstract: High-strength steels (HSSs) have been gaining increasing attention in recent years because of their potential application for lightweight structures. Hybrid structural steel I-sections, featured by dissimilar strength grades for constitutive plates, provide a more economical solution to suit bending loading scenario. This study conducted experiments on nine I-sections with Q690 flange plates under four-point loads, incorporating three different web strength grades including Q690, Q460, and Q355. Furthermore, the local buckling behavior of representative I-sections with various section geometries was analyzed using a validated numerical method to understand the role of web strength grade. Test and numerical analysis results revealed that the section with web steel in the strain hardening stage exhibited different levels of ductility among specimens with different strength webs. It was also observed that earlier yielding or inelastic buckling of the lower strength web plate in hybrid I-sections affects the local buckling behavior of I-girders, in terms of moment resistance and rotation capacity. In addition, the initial local imperfection mode used in numerical analysis was found to affect the rotation capacity of I-girders, but the effect of web strength grade remains consistent among I-sections with the same local buckling deformation mode. This study provides further insights into the local buckling behavior of hybrid I-sections subjected to uniform bending, laying the foundation for further development of design methods.

Author keywords: High-strength steel (HSS); Hybrid design; Local buckling behavior; Uniform bending.

Introduction

Because of the potential application for lightweight structures, high strength steel (HSS), characterized by a nominal yield strength $f_{y,nom}$ not less than 460 MPa, has gained increasing popularity these years. First conceptualized by Haaijer (1963), hybrid design, employing dissimilar strength grades for the constitutive plates of steel sections, offers more opportunities to maximize the material utilization under various loads. For I-sections under flexure, the higher strength steel is commonly selected for the flange plates, which contribute much more to the bending resistance than the web.

The earliest research on the local buckling behavior of hybrid I-section flexural members (i.e., I-beam or I-girder), in terms of cross-section resistance and rotation capacity, could date back to the 1960s in the United States. Frost and Schilling (1964) tested two hybrid I-beams with 50 ksi (≈345 MPa) and 33 ksi (≈230 MPa) carbon steel webs for which the flanges are made of 100 ksi (≈690 MPa) steels. It was concluded that the web yielding in hybrid I-beams at the bending moment when the flange initially or fully yields has limited impact on the bending behavior. Lew and Toprac (1967) performed tests on five hybrid slender-web I-girders comprised of A514 steel (nominal yield strength $f_{y,nom}$ = 690 MPa) flanges and A36 steel ($f_{y,nom}$ = 250 MPa) webs with varying flange and web thicknesses. Experimental observations showed that the transfer of stress from the web to the compression flange is limited because of web buckling. Based on the published research results, it was reported by the Joint AISC-AASHO Committee on Flexural Members (1968) that the design of hybrid I-section flexural members may simply be based on the flange-yield moment which causes the initiation of flange yielding, and the web yielding in hybrid sections can be disregarded. This statement lays the foundation of the hybrid design in American specifications since then, despite the fact that the American Institute of Steel Construction (AISC) has removed the provisions on the handling of hybrid built-up members for the design of structural steel buildings since the 2005 version-ANSI/AISC 360-05 (AISC 2005; White 2003). In the United Kingdom, Kamtekar et al. (1974) from the University of Cambridge also experimentally investigated the bending behavior of hybrid I-beams constituting Grade 55 flanges ($f_{y,nom}$ = 380 MPa) and Grade 43 webs ($f_{y,nom}$ = 275 MPa), and the beneficial effect of strain hardening developed in lower strength webs on the moment capacity was reported.

It was not until around 30 years later that the hybrid design of steel sections attracted renewed interest, resulting from the development of manufacturing technology. Shokouhian and Shi (2015) studied the flexural strength of hybrid I-beams with Q460 flanges ($f_{y,nom}$ = 460 MPa) and Q355 webs ($f_{y,nom}$ = 355 MPa) through testing, and a comprehensive strength prediction equation incorporating local and overall slenderness was proposed based on numerical analysis. Wang et al. (2016) explored the effect of slenderness as well as the strength grade of the constitutive plates on the bending behavior of hybrid I-girders through tests, of which the results showed that rotation capacity does not always increase proportionally with the web strength, and the web-to-flange yield strength ratio is suggested to be optimized for maximizing material utilization. More recently, Zhu et al. (2023) reported that hybrid I-girders undergo a gradual plastification of the web, leading to a diminished ability for providing rotational support to the flanges against local buckling.

To date, research on hybrid I-sections is relatively scarce, and there hasn't been a consensus on the role of the lower strength web in hybrid I-sections. Only the discussed literature mentioned above has experimentally examined the local buckling characteristics of hybrid I-sections under uniform bending, which is summarized in **Table 1**. From this table, it was found that the ratio of web to flange nominal yield strength (f_{yw}/f_{yf}) varies from 0.33 to 0.82, and specimens with flanges made from 690 MPa are rare. Note that AASHTO LRFD Bridge Design Specification (AASHTO 2020), which possesses the most detailed design provisions on hybrid sections, prescribes that the web yield strength f_{yw} shall not be less than 70% of flange yield strength f_{yf} and 36 ksi (≈250 MPa), whilst Eurocode 3 (CEN 2006a, b) stipulates that hybrid girder with $f_{yw}/f_{yf} \geq 0.5$ is allowed. This indicates that there is still a research need to clearly understand the effect of lower strength web in hybrid design.

In this study, a comprehensive experimental study on I-sections featuring Q690 flanges was performed to ascertain the effect of web strength grade on the local buckling behavior of a hybrid design. Nine I-beams with different web slenderness ratios were tested under uniform bending, including three web strength grades: Q690, Q460, and Q355. Through the numerical method validated with test data, I-section models with various moment-rotation characteristics were also analyzed to gain insights into the role of web strength in the local buckling behavior of hybrid I-beams.

Codified design methods for hybrid I-beams

For illustrative purposes, codified design methods for hybrid I-beams are first presented herein. **Table 2** tabulates the cross-section classification methodologies in the current American bridge specification and European design codes for the hybrid design of I-sections (AASHTO 2020; CEN 2005, 2006a, b, 2007). In this table, R_{cap}, as defined in **Fig. 1**, is the rotation capacity at moments between the first full yielding of the section (M=M_p) and the occasion when M drops to M_p; M_u is the ultimate (maximum) moment capacity; M_p and M_y represent the full plastic moment and yield moment of sections under flexure; E is the elastic modulus of the steel material. In **Fig. 1**, θ_p is the rotation defined as the ratio of M_p to the initial beam stiffness. In AASHTO specification, the moment distribution is only permitted for compact compression flanges, indicating the necessity for ductility in compact elements. This requirement is explicitly stated in the AISC specification (AISC 2022) as R_{cap}≥3. According to **Table 2**, it can be observed that the compact section as defined in the AASHTO specification is comparable to Class 1 as outlined in Eurocode 3, while the noncompact section aligns with Class 2 and Class 3. For hybrid sections, both AASHTO specification and Eurocode 3 state that the flange yield strength shall be used for the determination of web class.

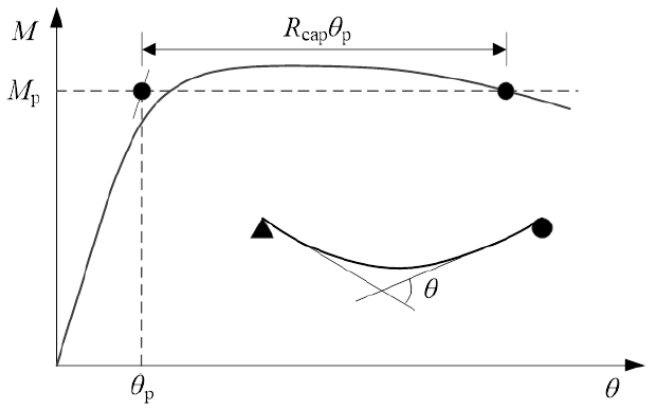

Fig. 1. Definition of rotation capacity

Table 2 also presents the codified limiting width-to-thickness ratios for compression elements in doubly symmetric I-sections with $f_{y,nom}$ up to 690 MPa subjected to flexure. This table shows inconsistencies between AASHTO specifications and Eurocode 3 regarding limiting slenderness ratios for flange and web plate elements. In the AASHTO specification, a hybrid factor R_h is introduced to account for the earlier yielding of the lower strength grade web in the hybrid section, as given by **Equation (1)**, where β is the ratio of web to flange areas, and ρ denote the web-to-flange yield strength ratio. The calculation of the yield moment for

hybrid I-sections $M_{y,HY}$ is illustrated in **Fig. 2**. In this figure, $M_{y,HO}$ represents the yield moment of a homogenous I-section with the same strength grades for the flange and web plates. The yield moment of a hybrid I-section with the same flange strength as the homogenous counterparts, can then be calculated by multiplying R_h by $M_{y,HO}$.

$$R_h = \frac{12 + \beta\left(3\rho - \rho^3\right)}{12 + 2\beta} \tag{1}$$

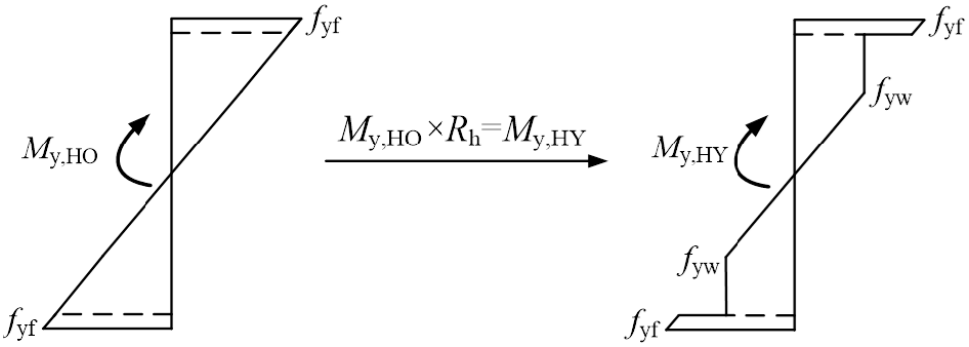

Fig. 2. Calculation of the yield moment for hybrid I-sections

Experimental Study

Test specimens

Nine four-point bending tests were carried out in this study. Three web strength grades-Q690 ($f_{y,nom}$ = 690 MPa), Q460 ($f_{y,nom}$ = 460 MPa), and Q355 ($f_{y,nom}$ = 355 MPa) were investigated for I-sections with Q690 flange plates. Therefore, two groups of hybrid I-sections with $f_{yw}/f_{yf} \approx 0.51$ and 0.67 were examined, along with their homogeneous HSS counterparts. Gas Metal Arc Welding (GMAW) was applied to connect the flange and web plates by 6 mm thick fillet welds with a gas mixture of 80% Argon and 20% carbon dioxide. Wire electrodes were selected to be in conformity with the material characteristics of the web plate to avoid cold cracking (Mvola, et al. 2016; Bayock, et al. 2019). Tensile coupons were extracted from the parent HSS plates to measure the material properties, and the measured material properties with detailed testing procedures are presented in Chen et al.(2023b). The average measured material characteristics are displayed in **Table 3**. In this table, f_y and f_u represent the yield strength and ultimate tensile strength; ε_y, ε_{sh} and ε_u denote the yield strain, the strain at the onset of strain hardening and the ultimate strain; "-F" and "-W" represent the steel plate employed for flange and web, respectively.

The flange of all the examined I-sections were designed to be compact/Class 1 in accordance with the American bridge specification and European codes, whilst three web width-to-thickness ratios were considered. The nominal width and thickness of flanges are 110 mm and 10 mm, and the nominal web thickness is 6 mm, with section depths of 310 mm, 350 mm, and 440 mm. **Fig. 3** illustrates the notation of I-section geometry, where $b_{f,t}$ and $b_{f,b}$ are the widths of top and bottom flanges; $t_{f,t}$ and $t_{f,b}$ represent the thickness of top and bottom flanges; H is the section height; h_f is the fillet weld leg size. The measured section geometry of I-beams, as well as the web classes determined based on American bridge specification and European codes are reported in **Table 4**. The specimen labeling implies the loading scenario, section height and web strength grade of I-beams, e.g., "4P-H350-460W" is a four-point loaded specimen with 350 mm section height, and the web is made of Q460 steel plate. From this table, it can be observed that the value of R_h decreases as the web strength grade lowers, which is consistent with the definition of hybrid factor R_h. The web slenderness of specimens in this study includes non-slender (i.e., compact and noncompact) webs defined in the AASHTO specification, and Class 2 to Class 4 webs defined in Eurocode 3.

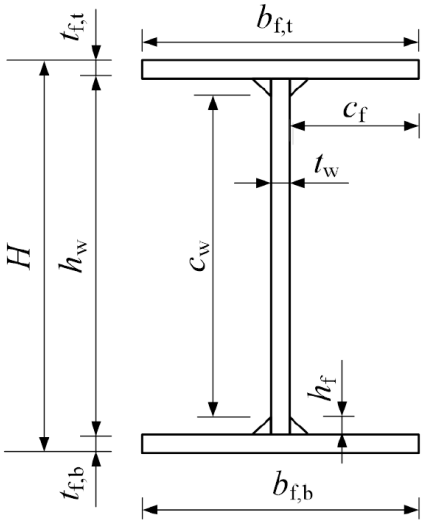

Fig. 3. Notation of I-section geometry

Test setup

The test setup for four-point loaded beams is outlined in **Fig. 4**. With the length L of 3,300 mm between end supports, four sets of rollers were adopted in four-point bending tests to ensure the loading remains symmetric as the beam deforms (Ziemian 2010), in which two rollers are located at the end supports and the remaining two rollers are placed at loading points [**Fig. 4(a)**]. A specially developed set of lateral restraints was used to

provide the desired lateral restraints at different positions on the beams, to prevent lateral torsional buckling, as illustrated in **Fig. 4(b)**. The uniform length L_c of specimens is designed to be 700 mm, and sufficient stiffeners were also welded onto the double-sized I-sections to prevent shear buckling. To minimize friction, 1 mm thick Teflon plates lubricated with grease were placed between the lateral restraints and beams. Two inclinometers were positioned at both ends of the beams to monitor the rotation of the beams. The four-point tests were conducted in the Structural Engineering Research Laboratory at The Hong Kong Polytechnic University. A 1,500 kN hydraulic cylinder with a manual pump was used, applying a load at a rate of approximately 10 kN/min. All the beam tests were anticipated to be stopped when the moment resistance of the specimens drops below M_p.

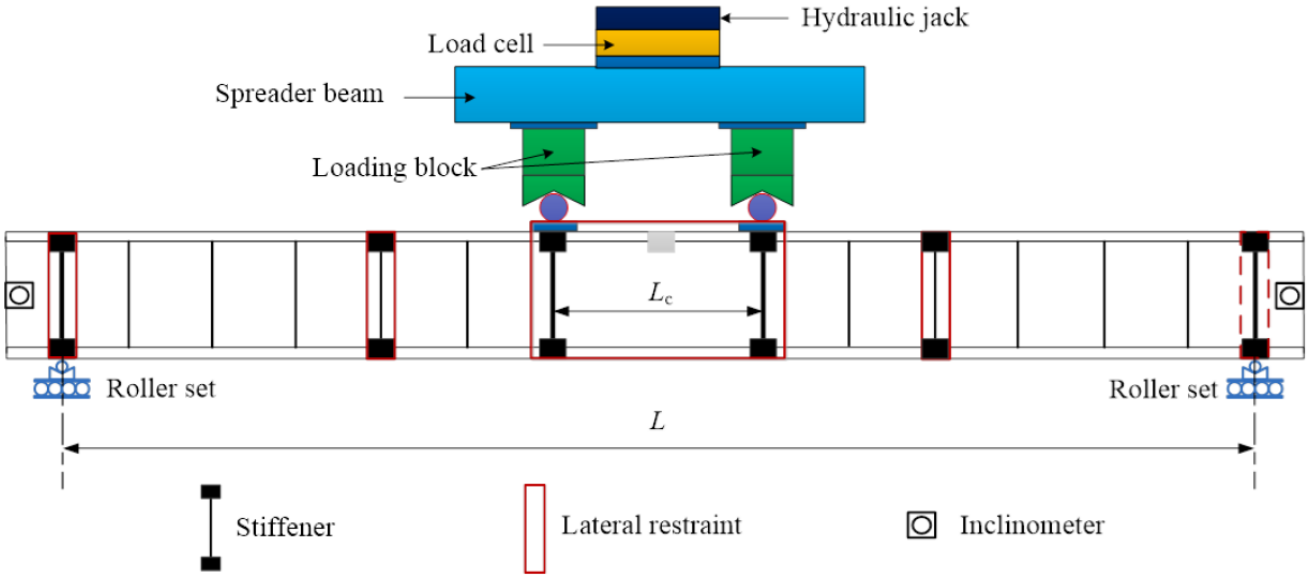

(a)

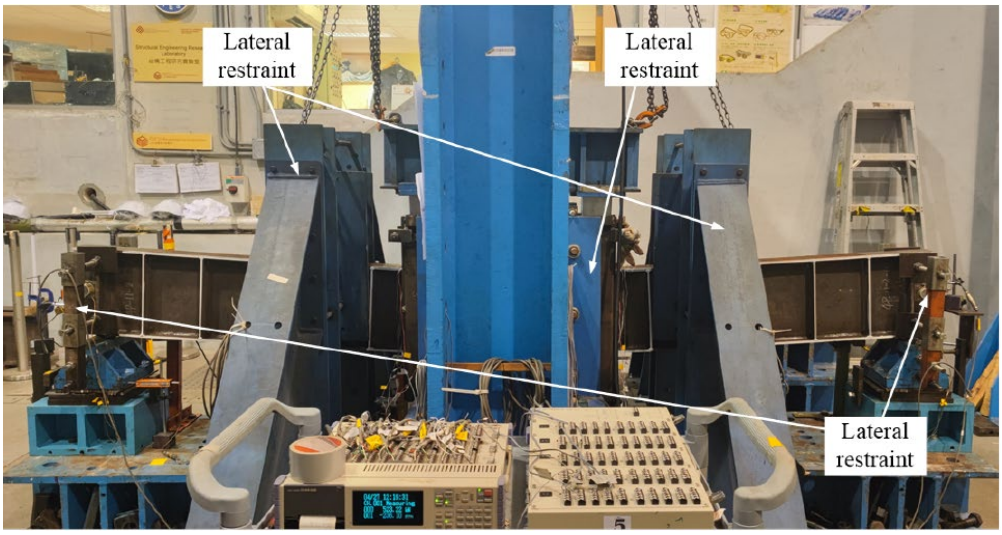

(b)

Fig. 4. Test setup of the four-point bending test: (a) schematic view of the four-point bending test; and (b) experimental arrangement with a beam specimen in place

Test results

Typical failure modes of the tested I-beams are depicted in **Fig. 5**, where the antisymmetric local deformation of flange and web plates was observed at the midspan of test specimens. Normalized moment-rotation curves of I-sections under uniform moment are shown in **Fig. 6**, with the moment-rotation characteristics values presented in **Table 5.** A relative rapid loading drops after achieving peak load was measured for the specimens of "4P-H310-690W" and "4P-H310-460W", principally attributed to the moderate sliding occurring between the loading block and spreader beam.

Fig. 5. Typical failure mode

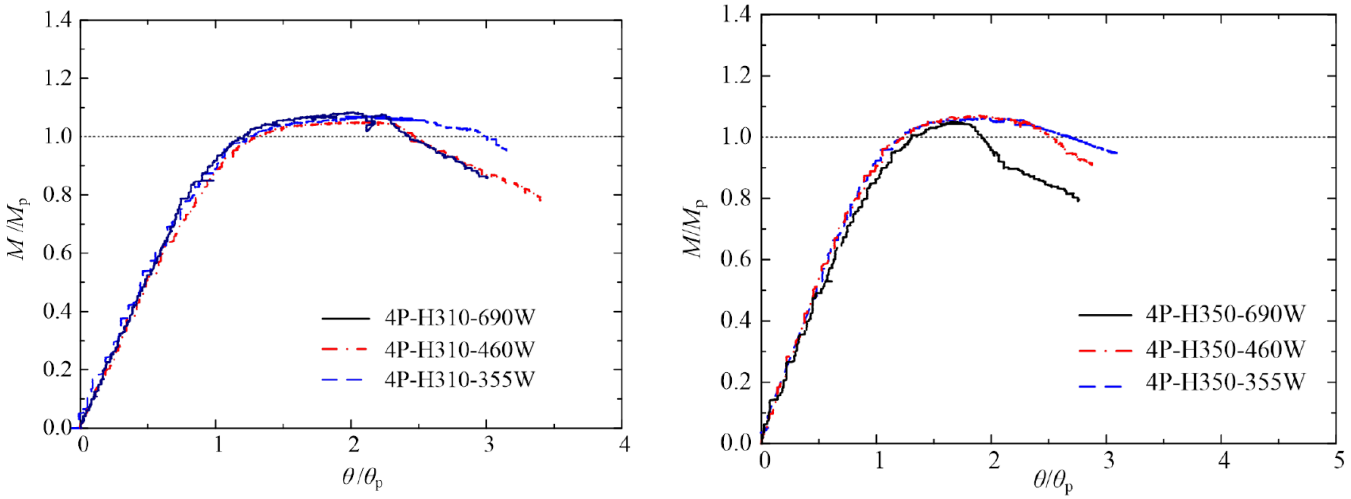

(a) **(b)**

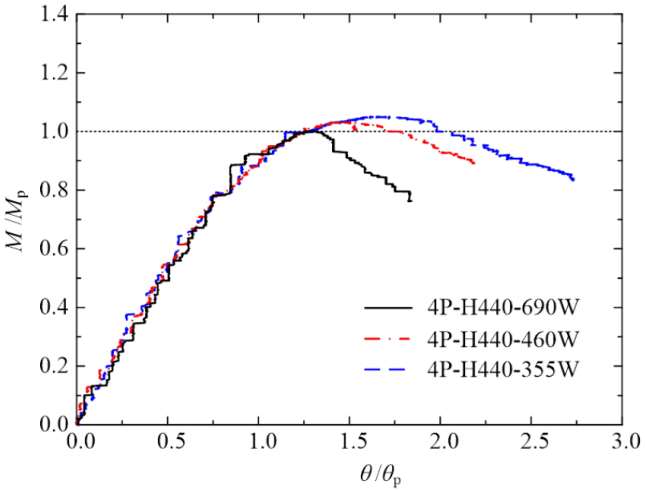

(c)

Fig. 6. Normalized moment-rotation curves of specimens: (a) "4P-H310" specimens; (b) "4P-H350" specimens; (c) "4P-H440" specimens

In **Fig. 6**, no obvious dispersion was found on the normalized moment capacity M/M_p among different web strength specimens, for which the section heights are 310 mm and 350 mm. For I-sections with 440 mm section height, it is apparent that the one with lower strength web exhibits greater values of M/M_p and better rotation capacity. These observations coincide with the experimentally obtained ultimate flexural strength $M_{u,test}$ in a normalized form of $M_{u,test}/M_p$ and ductility R_{cap} in **Table 5**. Additionally, it was observed that "4P-H310" and "4P-H350" specimens, which are defined as the compact section according to AASHTO specification, fail to meet the requirement of rotation capacity R_{cap} greater than 3. One potential reason may lie in the less pronounced strain hardening characteristic and decreased ductility of the HSS flange in comparison to conventional steel, as evidenced in Wang et al. (2016) that the rotation capacity of I-girders also partially attributed to the material characteristics of flange strength grade.

Finite element method analysis

Validation of finite element modelling

A numerical simulation tool-Abaqus 2019 (Dassault Systemes 2019) was used to further understand the effect of web strength grade on I-beams with various section geometry characteristics. The full-span modeling method established by Chen et al. (2022) was used to replicate the four-point loaded beam tests, as displayed in **Fig. 7**. The measured initial imperfections and residual stresses (Chen 2022) were input as initial states of

the models. The accuracy of the developed finite element (FE) modeling method was validated through comparisons of numerical and experimental test results for ultimate loads, moment-rotation characteristics, and failure modes. Experimental results were compared to the moment capacities obtained by the FE method in **Table 5**. The average ratio of FE method result $M_{u,FE}$ to the experimental test result $M_{u,test}$ is 0.969, with the highest and lowest values being 0.992 and 0.941, respectively. Furthermore, the corresponding Coefficient of Variation (CoV) of $M_{u,FE}/M_{u,test}$ is 0.017, indicating reliable and conservative predictions provided by the FE models. The good agreement in the normalized moment-rotation curves between tests and FE models of "4P-H310-355W", "4P-H350-355W" and "4P-H350-690W" is shown in **Fig. 8**, as well as the consistency of the typical failure mode in **Fig. 9** validates the effectiveness of the developed FE method.

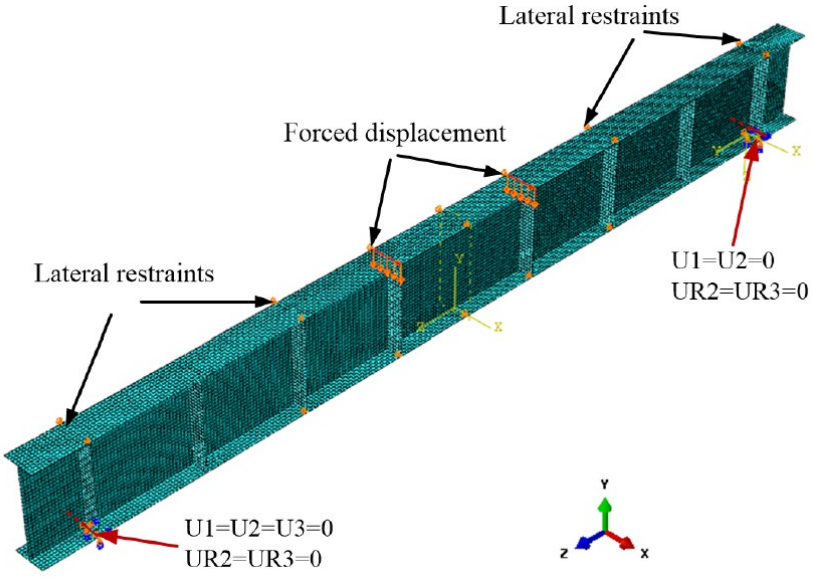

Fig.7. Full-span finite element model

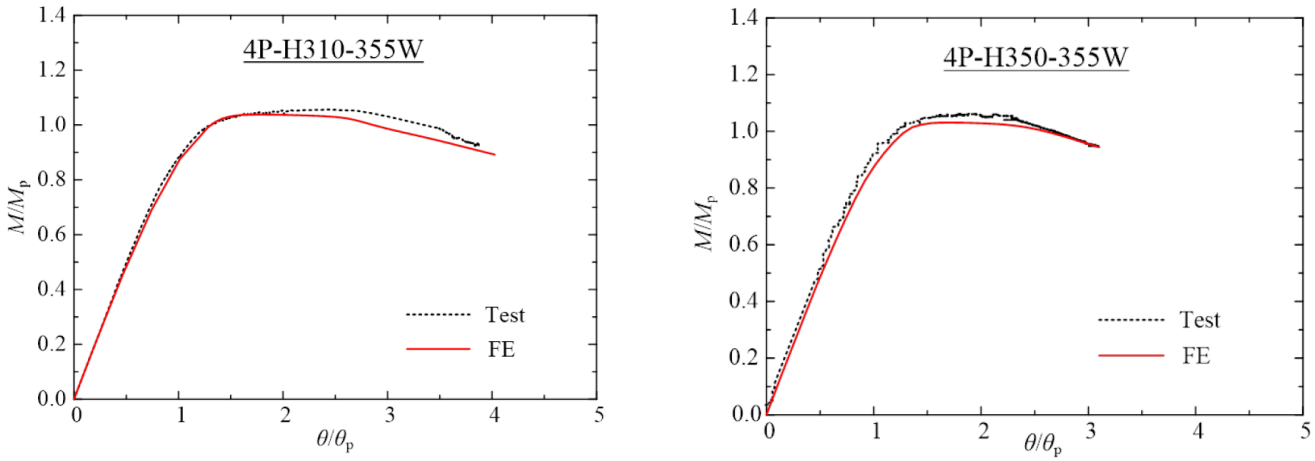

(a) **(b)**

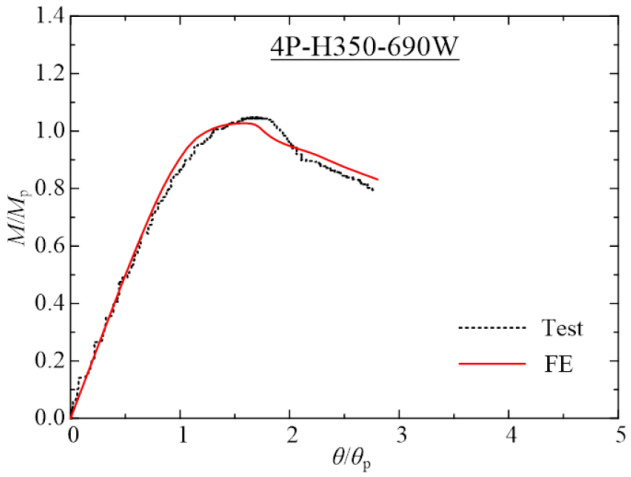

(c)

Fig. 8. Comparison of moment-rotation characteristics: (a) 4P-H310-355W; (b) 4P-H350-355W; (c) 4P-H350-690W

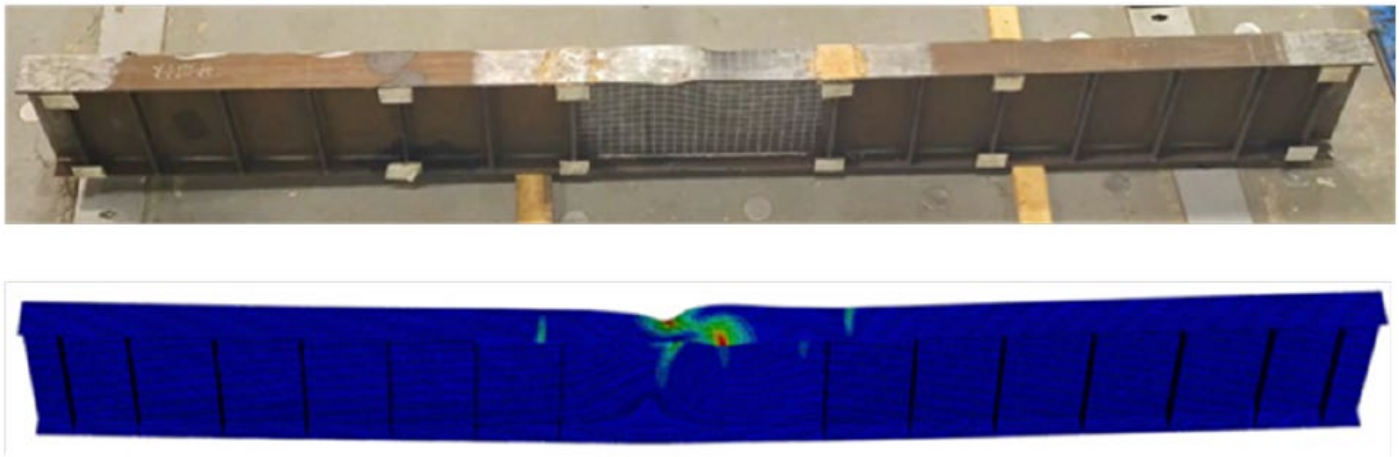

Fig. 9. Comparison of failure mode

Effect of web strength grade

In this study, representative I-sections with different section geometries were simulated to investigate the local buckling behavior of hybrid I-sections subjected to four-point loading. The length of the uniform moment was selected as three half-wavelengths of cross-section under four-point loading condition to easily observe the deformation behavior of plate elements at the mid-span. The determination of half-wavelength is based on prediction formulas proposed by Fieber et al. (2019), which can consider the mutual constraints between flange and web plates at the junction. Typically, the presence of initial welding-induced residual stress primarily accelerates the onset of local buckling in I-sections at the early stage but has a limited influence on

the moment-rotation characteristic of I-girders as demonstrated by Chen et al. (2024). Thus, the simulation of residual stress is not included in this study and the investigation concentrates on the role of web strength grade in the local buckling behavior of I-sections under uniform bending. The true stress-strain relationship displayed in **Table 6**, which is based on statistical analysis results from Yun and Gardner (2017) and Chen et al. (2022), was imported into FE models using multi-linear constitutive models. In this table, $f_{y,true}$, $f_{sh,true}$ and $f_{u,true}$ represent the true yield strength, the true strength at the onset of strain hardening, and the true ultimate tensile strength of steels; $\varepsilon_{y,true}$, $\varepsilon_{sh,true}$ and $\varepsilon_{u,true}$ are the true yield strain, the true strain at the onset of strain hardening and the true ultimate strain.

The geometrical characteristics of the selected representative I-sections are set out in **Table 7.** The thickness of flange and web is 10 mm and 6 mm. The designation of I-sections is in accordance with flange width and web height. These I-sections are categorized into three series according to their moment and rotation capacities, with the critical plate element for I-sections under flexure, the flange and web classes in accordance with AASHTO and Eurocode 3. The critical plate members, governing the local buckling behavior of cross-sections, is defined as the one with lower elastic buckling stress with simply supported unloaded edges (Gardner et al., 2019; Chen et al., 2023a).

In this section, the specified local geometrical imperfection magnitude as outlined in EN 1993-1-5 (CEN 2006a) is used with the first-eigenmode shape determined through "BUCKLE" analysis under four-point loading condition. For I-girders with web as the critical plate element, the value of $h_w/200$ is taken as the local geometrical imperfection amplitude; whilst for those flange-critical I-sections, the magnitude of $c_f/50$ is applied.

The elastic critical local buckling moment M_{cr} of representative I-sections is given in **Table 8**, where $M_{cr,Gardner}$ and $M_{cr,FE}$ denote the results determined from the estimation method as per Gardner et al. (2019) and eigenvalue buckling analysis through FE method, respectively. It can be seen that the ratio of $M_{cr,Gardner}$ to $M_{cr,FE}$ falls between 0.95 and 1.01, demonstrating the high accuracy of Gardner's method. The values of M_{cr} for these models are utilized in the subsequent subsections to ascertain that there is elastic or plastic local buckling occurring in sections.

I-sections with $M_u > M_p$

Table 7 shows that the flange and web plates of all the I-sections with $M_u > M_p$ are classified as compact and Class 1 elements according to the AASHTO specification and Eurocode 3, respectively. Among these I-sections, the B40H100 models, have the most compact flange and web plates. **Fig. 10** compares the stress contour plots of the compression flange and web plates for web-critical B40H100 models at $M=M_u$. From this figure, it can be observed that the stocky flange of all three models reaches the true ultimate stress $f_{u,true}$ of Q690 flange steel ($f_{u,true}$ = 875.3 MPa). For the web plates, the zone reaching $f_{u,true}$ of the "Q690W" model is larger than that of the Q460 web ($f_{u,true}$ = 702.6 MPa), while the entire web plate of the model characterized by Q355 web ($f_{u,true}$ = 651.5 MPa) is still in the strain hardening stage. These differences can be attributed to the different strain hardening ranges of the web steels.

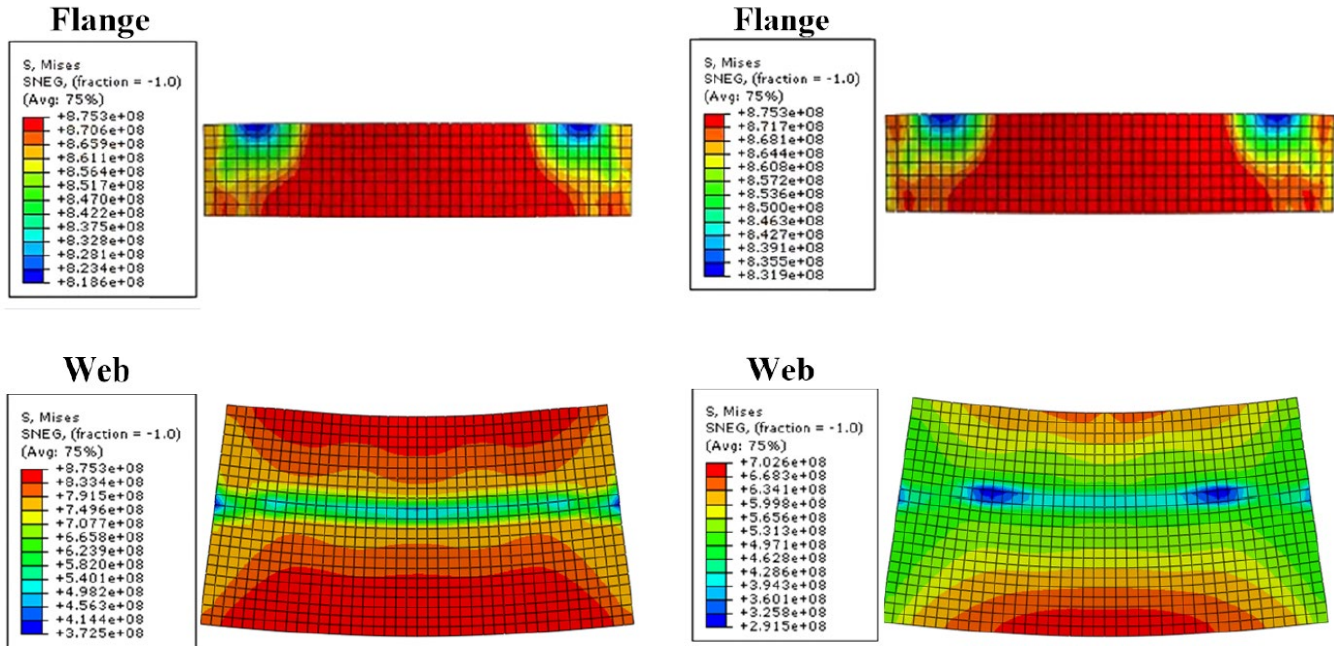

(a) **(b)**

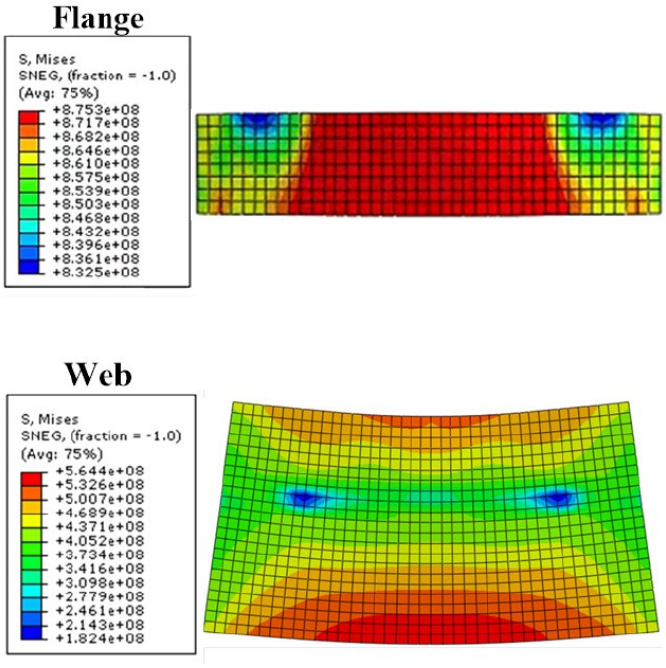

(c)

Fig. 10. Stress contour plots of B40H100 models (unit: N/m^2): (a) 690W; (b) 460W; and (c) 355W

In comparison to "B40H100" models, "B80H100" models are flange-critical sections with less compact flange plates, resulting in earlier buckling compared with stocky counterparts. The stress contour plots of the web plate for the B80H100 I-sections are shown in **Fig. 11**. Among them, the maximum stress of the web plate is close to its $f_{u,true}$ for "Q690W" model, while the maximum stresses of "Q460W" and "Q355W" models are still far from their corresponding $f_{u,true}$ values. Although the strength of the web has been found to impact the stress distribution of "B40H100" and "B80H100" I-sections, the significant plasticity of the flanges, which greatly contributes to their bending capacity, leads to no noticeable difference in the normalized moment M/M_p-rotation θ/θ_p curves among sections with different web strengths, as illustrated in **Fig. 12** and **Table 9**.

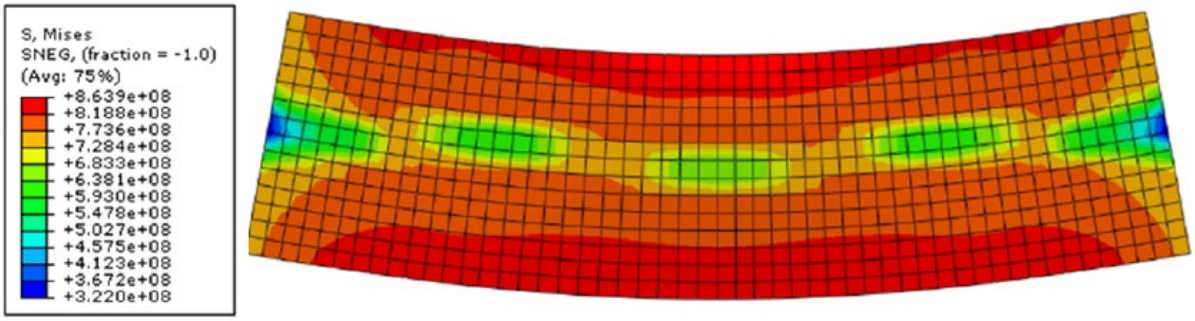

(a)

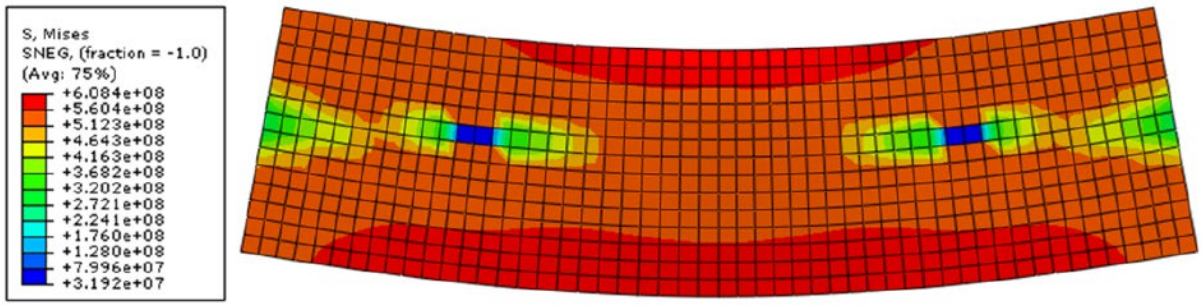

(b)

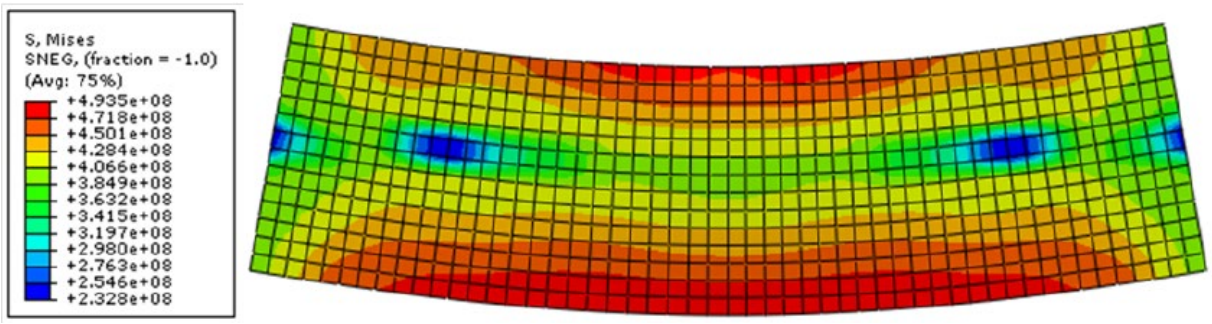

(c)

Fig. 11. Stress contour plots of B80H100 models (unit: N/m^2): (a) 690W; (b) 460W; and (c) 355W

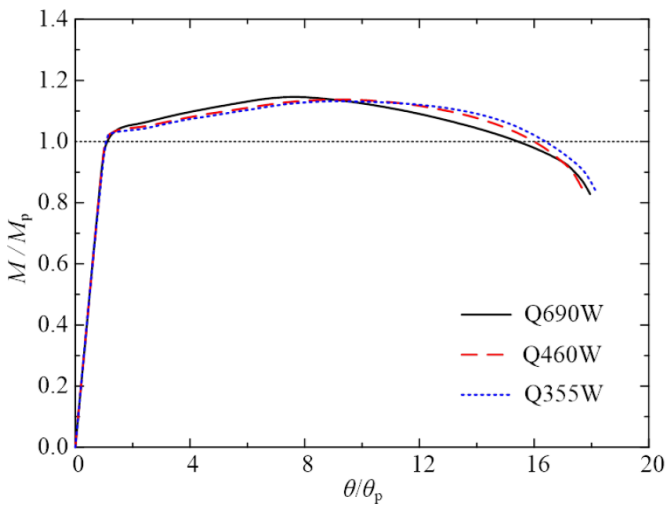

(a)

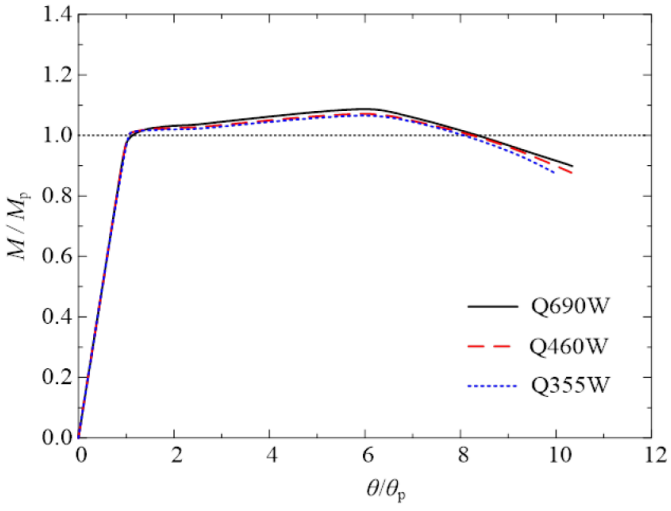

(b)

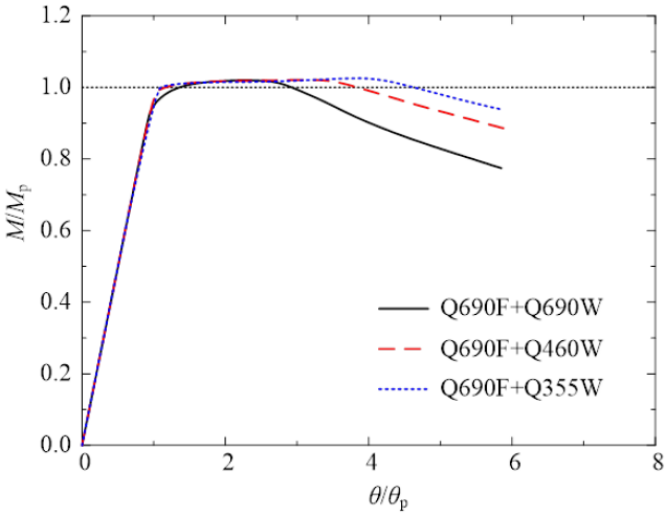

(c)

Fig. 12. Normalized moment-rotation curves for I-sections with $M_u > M_p$: (a) B40H100; (b) B80H100; and (c) B80H200

In **Fig. 12(c)**, a distinction is observed in the rotation capacity of "B80H200" models that the model with Q355 web presents the most favorable ductility. **Fig. 13** shows the stress contour plots of their compression flange and web plates at $M=M_u$. With the web being more critical than the flange, it can be observed from this figure that the stress-strain relationship of the web plate significantly influences the plasticity of the flanges. Among the B80H200 I-sections with different web strength grades, the compression flange of the "Q355W" model exhibits the most severe plastic deformation. This is consistent with the stress development observed in the web plates, where the Q355 web undergoes a greater strain hardening stage compared to the Q690 and Q460 webs. The difference can be explained by the crucial role played by the distinctive strain hardening characteristics of the Q355 web. This occurs when the geometry of the I-section causes the web to be in the early strain hardening stage at $M=M_u$. This result suggests that the limiting slenderness ratios used to distinguish between Class 1 and Class 2 in Eurocode 3 might take into consideration the web strength grade for hybrid I-beams.

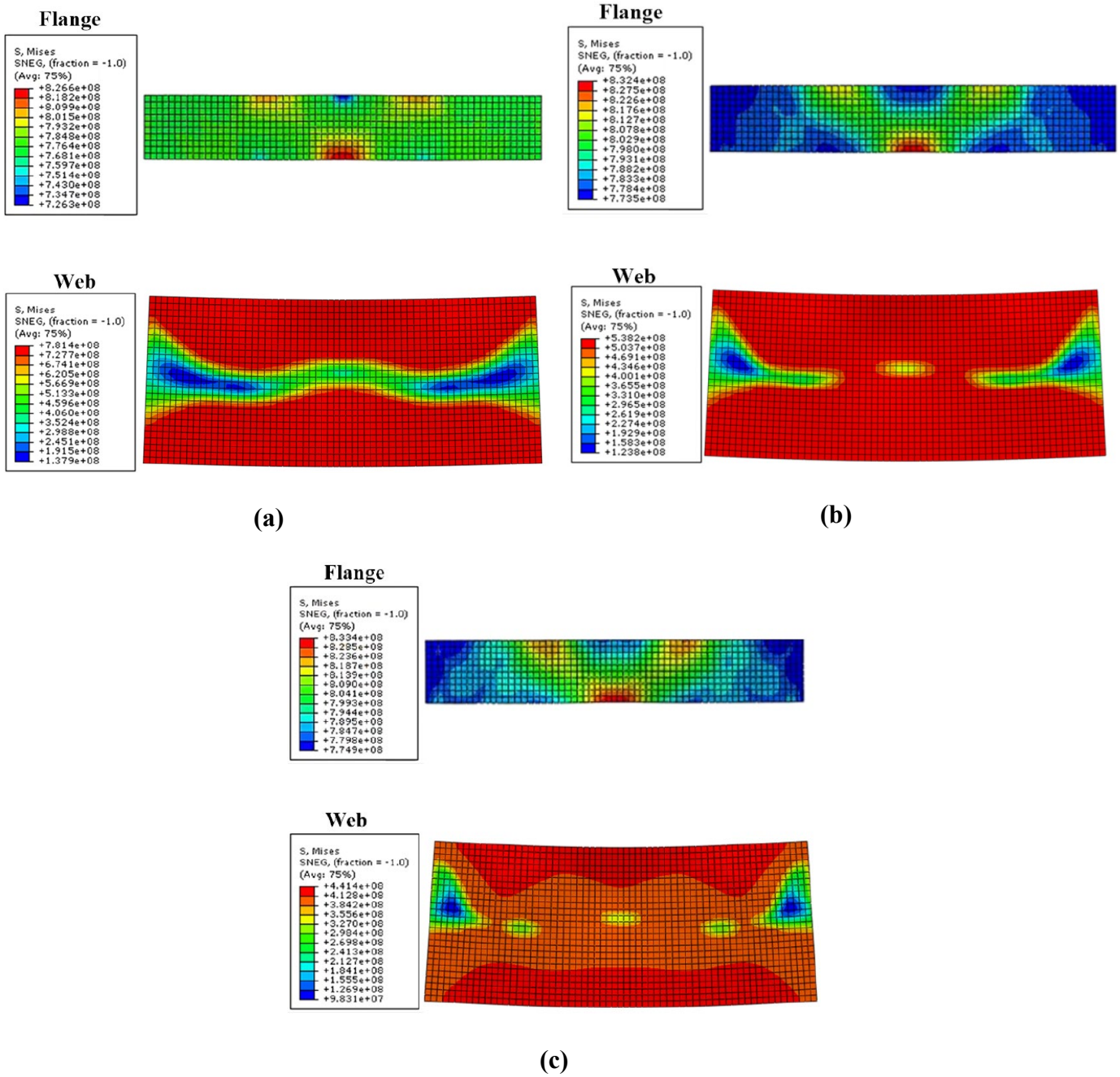

Fig. 13. Stress contour plot of B80H200 model (unit: N/m^2): (a) 690W; (b) 460W; and (c) 355W.

I-sections with M_p>M_u>M_y

"B160H200" and "B120H40" models are selected to investigate the deformation behavior of representative I-sections with M_p>M_u>M_y. Their moment M-web lateral deformation δ_w curves are depicted in **Fig. 14** to capture the web local buckling behavior, with the deformation measurement point located at 3/4 of the web height at midspan. **Table 7** shows that "B160H200" models are flange-critical sections, whereas "B120H400" models are web-critical ones. In **Fig. 14**, noticeably different transitions are observed in the M-δ_w of

"B120H400" models, whilst no distinction is observed among "B160H200" models until reaching the plateau stage. Since the critical local buckling moment M_{cr} of the "B120H400" models exceeds 900 kN×m (**Table 8**), which is significantly higher than their moment resistance, this suggests that the turning point in the M-δ_w curve signifies the onset of inelastic buckling in the web. The yield moment of the homogeneous I-sections made of Q690, Q460 and Q355 steels (denoted as $M_{y,Q690F+W}$, $M_{y,Q460F+W}$ and $M_{y,Q355F+W}$) is also highlighted in **Fig. 14(b)**. It can be observed that the values of $M_{y,Q460F+W}$ and $M_{y,Q355F+W}$ correspond to the turning points in the curves of "B120H400" hybrid I-sections with Q460 and Q355 webs, respectively. This implies that for the two hybrid I-sections, once the web experiences plastic buckling, their moment capacities primarily attributed to the contribution of much more compact flanges, which have higher strength than the web.

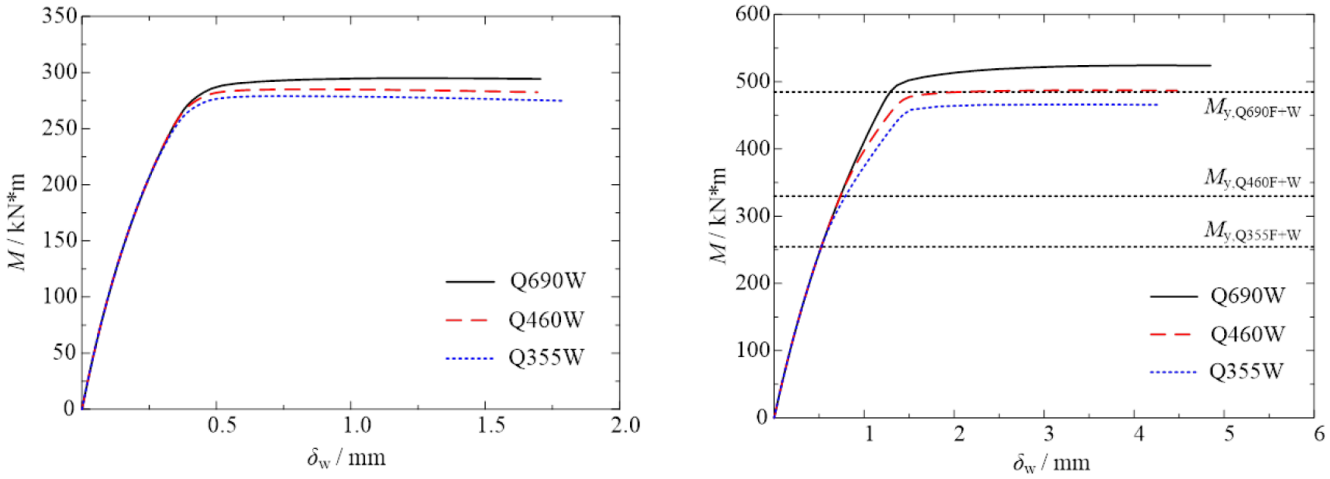

Fig. 14. Moment-web lateral deformation curves of I-sections with $M_p > M_u > M_y$: (a) B160H200; and (b) B120H400

In addition, the web inelastic lateral deformation of "B160H200" and "B120H400" models is displayed in **Figs. 15** and **16**, respectively. It can be seen in **Fig. 15** that for the "B160H200" model, the web plate of the homogeneous Q690 I-section shows a buckled shape caused by the flanges [**Fig. 15(a)**]. On the other hand, both hybrid I-sections [**Figs. 15(b)** and **(c)**] also exhibit uniform plastic development in the web near the flange-web junction. This is mainly due to the difference of strength grade between the flanges and the web in hybrid I-sections, by which the lower strength web enters the plasticity earlier. For "B120H400" models (**Fig. 16**), such uniform plastic distribution as seen in "B160H200" models is not observed due to the occurrence of web plastic buckling mentioned earlier. However, it can still be noticed that the web with the

lowest strength exhibits the most severe lateral plastic deformation, which occurs earliest, as presented in **Fig. 14(b)**.

The ultimate moment M_u was normalized by both M_p and M_y for "B160H200" and "B120H400" I-sections and the normalized magnitude is listed in **Table 9**. It was found that as the web strength grade lowers, the value of M_u/M_p increases whereas the value of M_u/M_y decreases. This could be explained by the fact that a larger area of the web plate undergoes plastic deformation for the lower strength web (**Figs. 15** and **16**), which is closer to the full plastic stress distribution of the I-section.

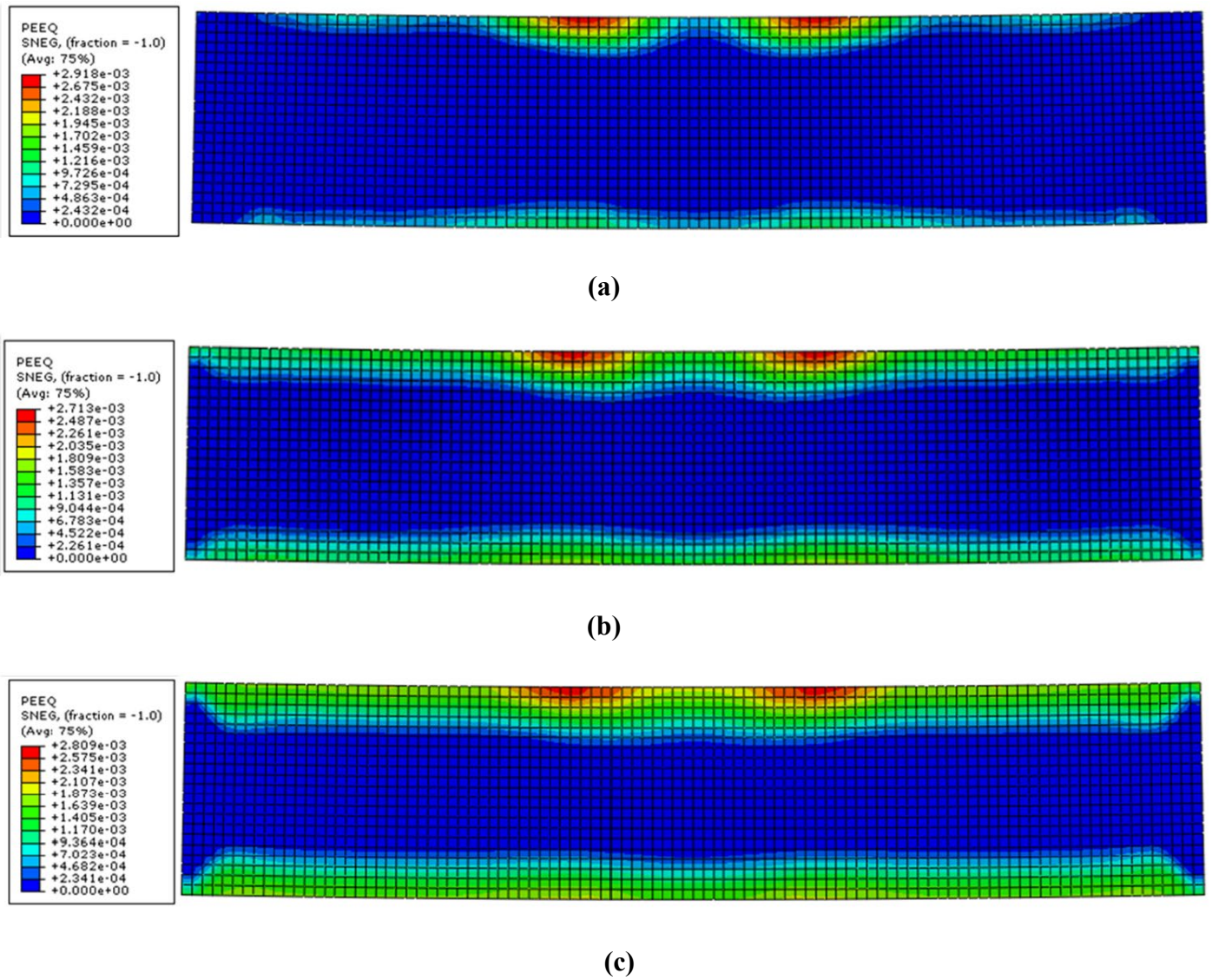

Fig. 15. Web inelastic deformation behavior of B160H200 models: (a) 690W; (b) 460W; and (c) 355W

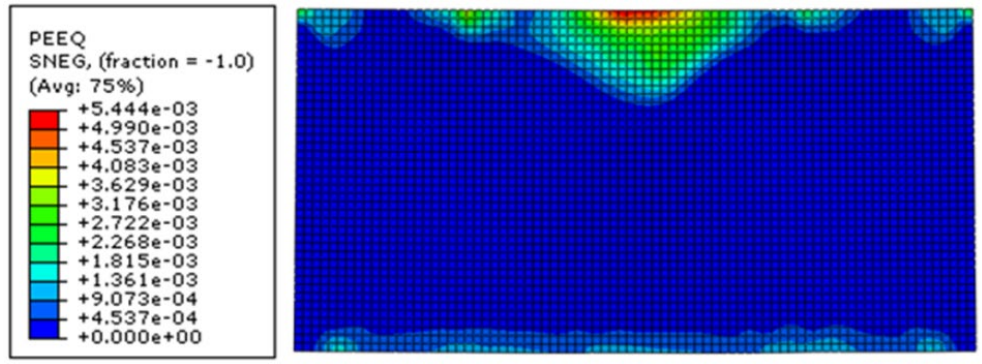

(a)

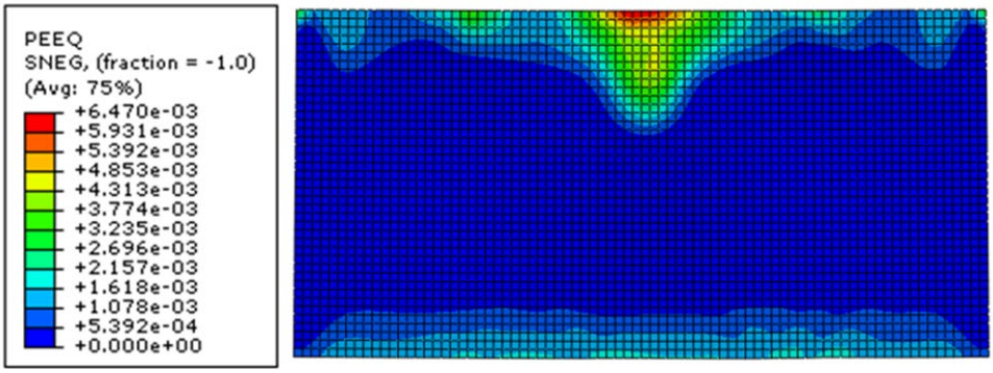

(b)

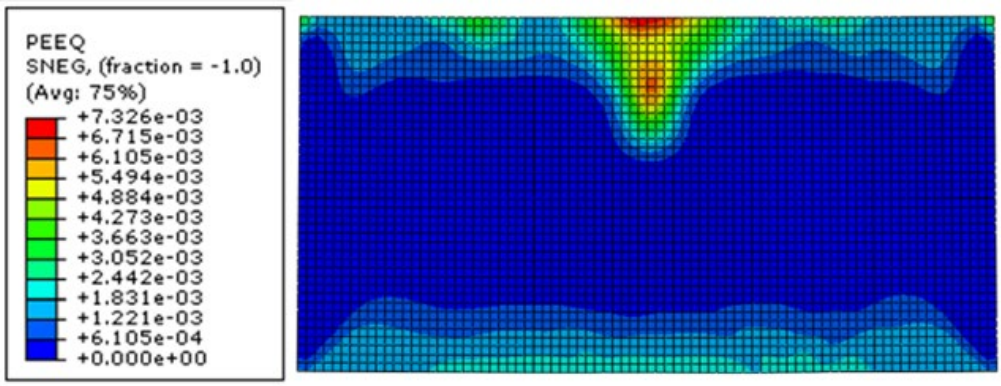

(c)

Fig. 16. Web inelastic deformation behavior of B120H400 models: (a) 690W; (b) 460W; and (c) 355W

I-sections with $M_u < M_y$

Among the selected I-sections with $M_u < M_y$, the critical plate element is the web for "B220H600" sections and the flange for "B340H600" models. **Fig. 17(a)** shows the moment M-web lateral deformation δ_w of "B220H600" models, together with the yield moment of homogeneous I-sections made of Q690, Q460 and Q355 steels (labelled as "$M_{y,Q690F+W}$", and "$M_{y,Q460F+W}$" and "$M_{y,Q355F+W}$" respectively). Similar to "B120H400"

models, the turning points of hybrid I-sections with Q460 and Q355 webs accord with the values of "$M_{y,Q460F+W}$" and "$M_{y,Q355F+W}$", indicating the occurrence of inelastic buckling in these webs due to their lower strength grades. Meanwhile, the ultimate moment M_u of homogenous Q690 I-sections is lower than $M_{y,Q690F+W}$, but greater than the elastic local buckling moment obtained by FE method-$M_{cr,FE}$, suggesting that the Q690 web experiences elastic buckling.

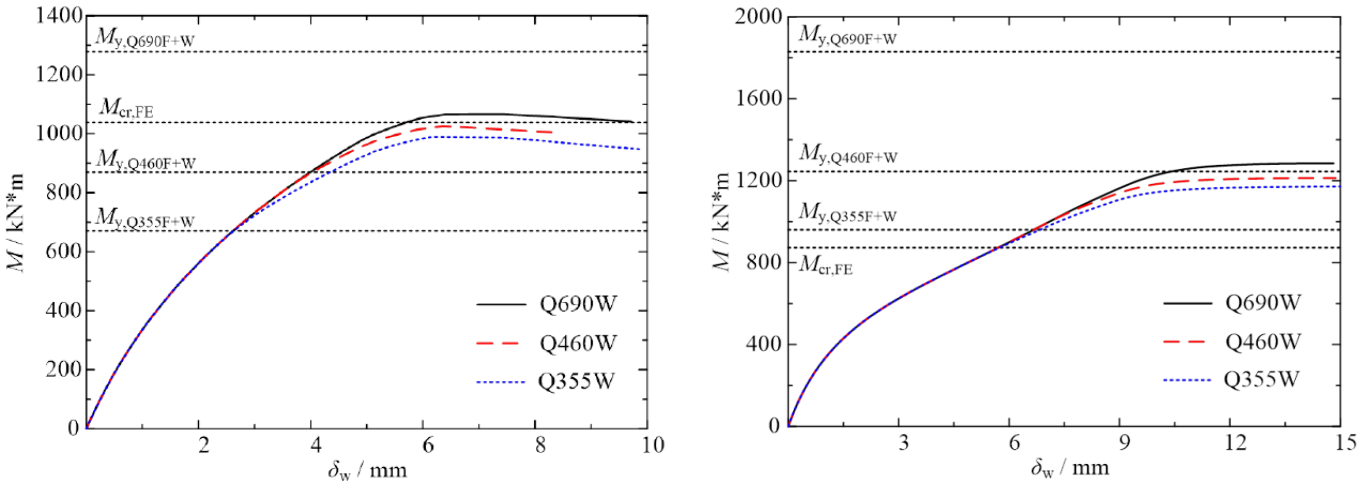

Fig. 17. Moment-web lateral deformation of I-sections with $M_u < M_y$: (a) B220H600; (b) B340H600

In comparison, it can be seen from the M-δ_w curves of "B340H600" I-sections [**Fig. 17(b)**] that the value of $M_{cr,FE}$ is lower than the ultimate moment of all three models with different web strength grades. As a result, the web plate of all the "B340H600" models experiences elastic buckling. This is demonstrated by the simultaneous transition of the curves at M=$M_{cr,FE}$ in **Fig. 17(b)**, rather than being governed by the yield moment M_y. However, it is worth noting that the deformation development after buckling of web plates is still slightly affected by the web strength grades. This is evidenced by the divergence among the curves above M=$M_{cr,FE}$ in **Fig. 17(b)**, as well as the difference in the degree of plastic deformation of these models shown in **Fig. 18**.

The normalized moment capacity M/M_y of "B220H600" and "B340H600" models is provided in **Table 9**. The same regularity is observed for M/M_y value varied with web strength grade, as in the case of I-sections with M_p>M_u>M_y, i.e., the value of M/M_y decreases with a lower strength grade.

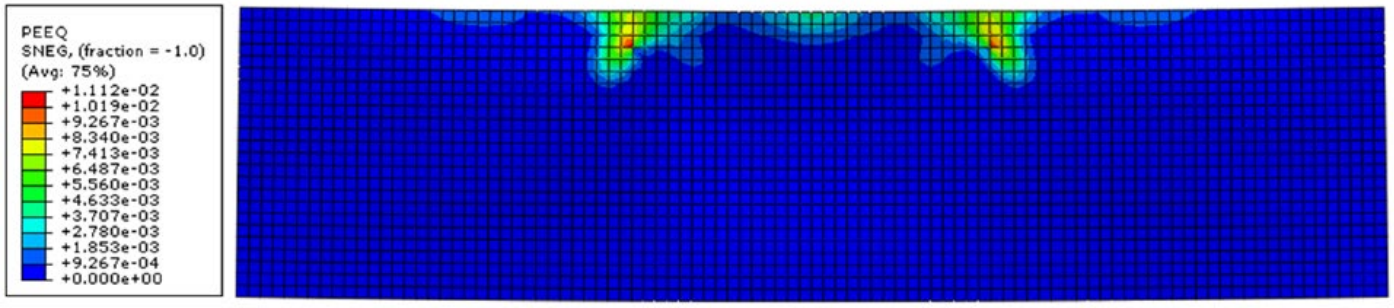

(a)

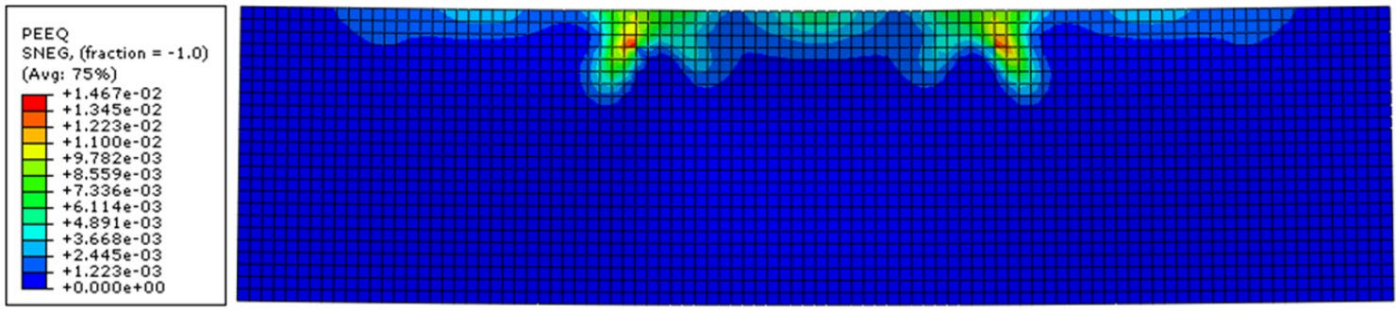

(b)

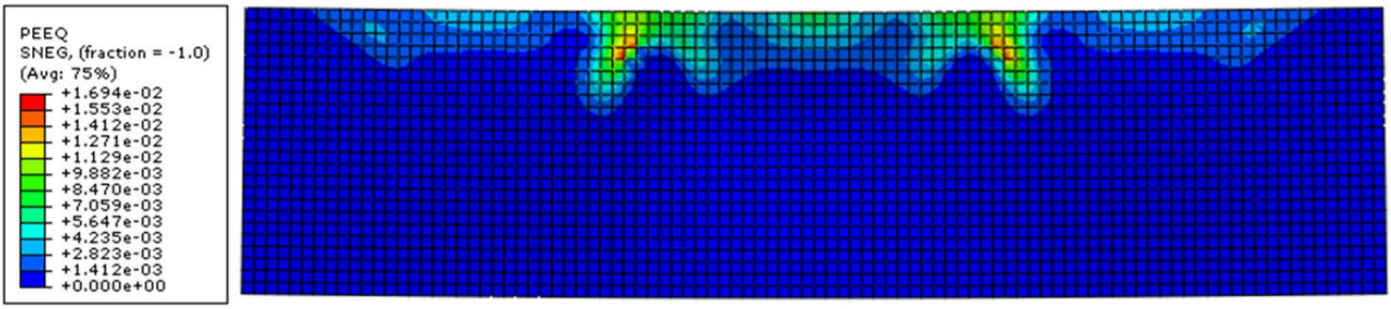

(c)

Fig. 18. Web plastic deformation behavior of B360H600 models: (a) 690W; (b) 460W; (c) 355W

Summary

In this section, the effect of web strength grade on the local buckling behavior of I-sections under uniform bending is analyzed using the validated numerical method. Based on the moment-rotation characteristics of representative I-section models, the following findings can be observed:

1. For I-sections with $M_u > M_p$: when the plate elements of I-sections are stocky enough, such that the flange plate can reach its material ultimate stress, the web strength grade has a negligible impact on the normalized moment and rotation capabilities; but when the plate elements are relatively slender

and the web is in the early stage of material strain hardening, the strength grade of the web becomes more significant, suggesting that the limiting slenderness ratios used to distinguish between Class 1 and Class 2 in Eurocode 3 might consider the web strength grade for hybrid I-beams.

2. For I-sections with $M_p > M_u > M_y$: the lower strength grade web commonly exhibits more severe plasticity due to earlier material yielding or inelastic buckling. The normalized ultimate moment M_u/M_p of these I-sections increases as the web strength decreases, while the opposite trend occurs in the normalized ultimate moment M_u/M_y.
3. For I-sections with $M_u < M_y$: hybrid I-sections may experience web inelastic local buckling, while the web of homogeneous counterparts buckles elastically. For these I-sections, the normalized moment M/M_y decreases as the web strength grade decreases.

Effect of initial geometrical imperfection

The study conducted by Gerard et al. (2019) comprehensively investigated the impact of local geometrical imperfection pattern (i.e., first buckling mode shape and sinusoidal functions) and magnitudes on the cross-section resistance of I-sections made of conventional steels. This study focuses on the effect of initial geometrical imperfection on the rotation capacity of compact I-sections with $M_u > M_p$ (i.e., "B40H100", "B80H100" and "B80H200" models). In addition to the local buckling deformation mode shape achieved from the four-point loading scenario (shown in **Fig. 7**) discussed in the preceding section, the first eigenmode shape under axial compression, where the susceptibility to local buckling of plate elements varies, was also incorporated for comparison to illustrate the impact of imperfection mode on rotational capacity of I-girders. The boundary condition and first buckling mode shape under axial compression by linear eigenvalue analysis in ABAQUS are illustrated in **Fig. 19**. In this figure, the forced displacement applied at both beam ends, for which only longitudinal displacement is allowed, and lateral restraints are also set to exclude the occurrence of global buckling.

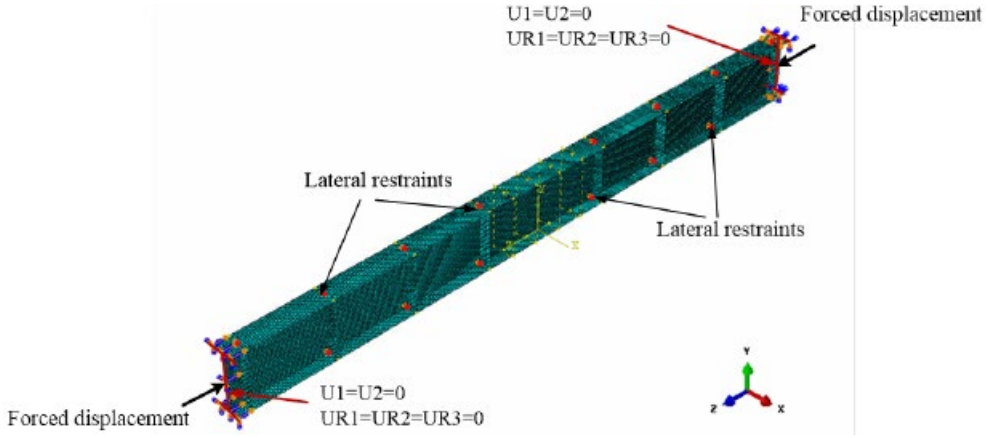

(a)

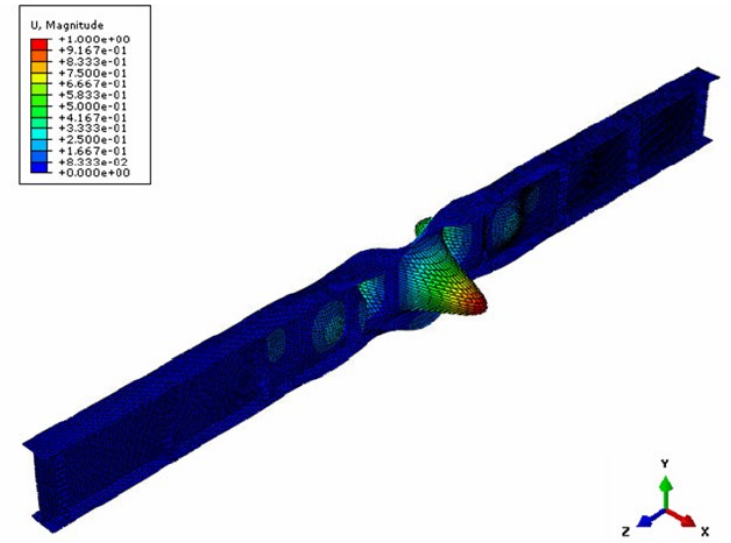

(b)

Fig. 19. Initial geometrical imperfection under axial compression: (a) boundary condition; and (b) first local bucking deformation mode

The magnitude of local buckling deformation mode under axial compression is determined to ensure the maximum deformation value of critical plate element of I-girders corresponds to the one suggested by EN 1993-1-5 (CEN 2006a). **Table 10** tabulates the local imperfection magnitude obtained through four-point loading and axial compression. In this table, $e_{f,max}$ and $e_{w,max}$ represent the local deformation amplitude of flange and web plates, respectively. In **Table 10**, the ratio of $e_{f,max}$ to $e_{w,max}$ is significantly higher under axial compression compared to four-point loading. This suggests that the boundary condition of axial compression makes the web plate more susceptible to local buckling. When the local imperfection magnitude is determined based on the same principle (i.e., the equivalent local imperfection magnitude recommended by Eurocode 3),

the difference in the value of $e_{f,max}$ or $e_{w,max}$ results from the loading condition of linear eigenvalue analysis, which is used for obtaining the initial local buckling deformation mode. Seen from this table, in the web-critical "B40H100" and "B80H200" models, the lower value of $e_{f,max}$ is obtained under the loading condition of axial compression, whereas the higher value of $e_{w,max}$ is observed under axial compression for flange-critical "B80H100" I-sections.

Fig. 20 illustrates a comparison of the moment-rotation curves of I-girders featuring $M_u > M_p$ with the initial geometrical imperfection obtained under various boundary conditions. In this figure, "-UM" and "-COM" represent the boundary conditions of four-point loading and axial compression, respectively. The failure mode of I-girders at the moment M dropping to M_p is also depicted in **Fig. 20**. It can be seen that the initial local imperfection has a minimal impact on the rotational capacity of the stockiest I-sections- "B40H100". In contrast, for the I-sections of B80H100 and B80H200, which exhibit a distinct inelastic local buckling failure mode, a larger magnitude of initial imperfection result in reduced ductility for the I-girders. Nevertheless, it is important to recognize that the effect of web strength grade is observed to be similar in one series of models using the same local imperfection mode. For example, although the B80H200 models with initial local imperfections determined under axial compression generally experience inferior rotation capacity, a similar trend is noted in I-sections with lower strength grades displaying enhanced ductility.

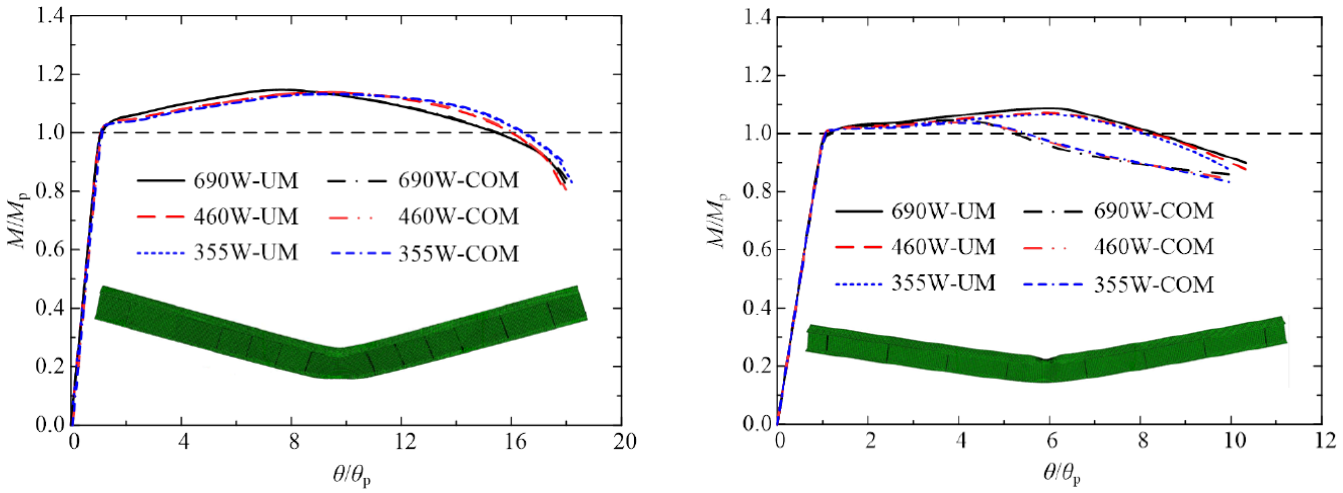

(a) **(b)**

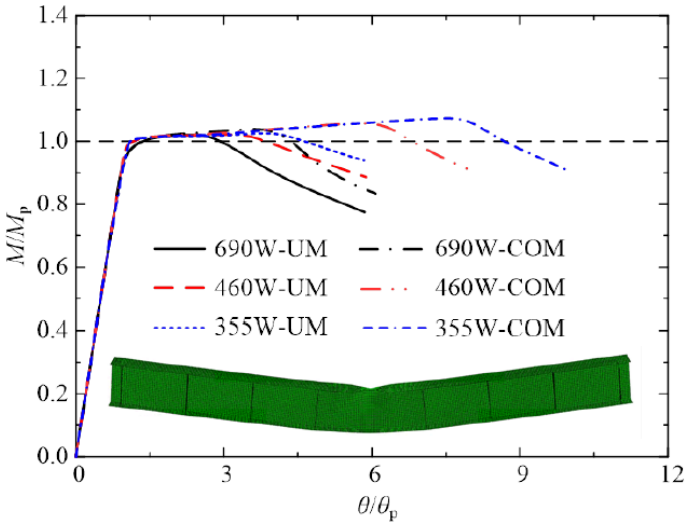

(c)

Fig. 20. Effect of initial geometrical imperfection: (a) B40H100; (b) B80H100; and (c) B80H200

Conclusions

In this study, to investigate the local buckling behavior of hybrid I-sections under uniform moment, nine I-beams with Q690 compact flanges with varying web strength grades and web slenderness were tested under four-point loading. Two groups of hybrid sections featured with Q460 and Q355 webs were studied, as well as homogenous HSS Q690 counterparts. It was shown from the moment-rotation characteristics of test specimens that I-sections with compact webs show the comparable normalized moment capacity M=M_p, while for specimens with noncompact webs, the I-sections with lower strength webs present higher values of M=M_p and better ductility.

In addition, to better understand the effect of web strength grade on the local buckling behavior of I-girders, representative I-sections with different moment-rotation characteristics are analyzed using a numerical method. The early yielding or inelastic buckling of the web plate in hybrid I-sections is found to undeniably affect the local buckling behavior of I-girders. Based on the analysis results, it is suggested that the AASHTO specification's limiting slenderness ratios used to distinguish between compact and noncompact, and the slenderness limit between Class 1 and Class 2 in Eurocode 3, might consider the web strength grade for hybrid I-beams. Also, the normalized moment capacity of I-beams which failed to achieve the full plastic moment was found to be influenced by web strength grades. Moreover, it is found that the choice of the initial local

imperfection mode influences the rotation capacity of compact I-sections failed by inelastic local buckling. However, the effect of web strength grade remains consistent among I-sections that adopt the same local buckling deformation mode. This study provides insight into the local buckling behavior of hybrid I-sections subjected to uniform bending, laying the foundation for further investigation of design methods that take the contribution of web strength grade in I-sections into account.

Data availability statements

Some or all data, models, or code that support the findings of this study are available from the corresponding author upon reasonable request.

Acknowledgments

The funding support from the Chinese National Engineering Research Centre for Steel Construction (Hong Kong Branch) at The Hong Kong Polytechnic University is gratefully appreciated. The authors would also like to acknowledge the technicians, Mr. C. F. Cheung, Mr. M. C. Ng and Mr. K. L. Cheung of the Structural Engineering Research Laboratory, and Mr. H.Y. Leung of the Mechanical Workshop at The Hong Kong Polytechnic University for their help on the experimental work.

References

AASHTO (American Association of State Highway and Transportation Officials). 2020. *AASHTO LRFD Bridge Design Specification*, 9th Ed. Washington, DC: AASHTO.

AISC (American Iron and Steel Institute). 2005. *Specification for Structural Steel Buildings*. ANSI/AISC 360-05. Chicago: AISC.

AISC (American Iron and Steel Institute). 2022. *Specification for Structural Steel Buildings*. ANSI/AISC 360-22. Chicago: AISC.

Bayock, F.N., P. Kah, B. Mvola, and P, Layus. 2019. "Experimental review of thermal analysis of dissimilar welds of high-Strength Steel." *Rev. Adv. Mater. Sci.* 58: 38–49.

CEN (European Committee for Standardization). 2005. *Design of steel structures, part 1.1: General rules and rules for buildings*. Eurocode 3. EN 1993-1-1. Brussels, Belgium: CEN

CEN (European Committee for Standardization). 2006a. *Design of steel structures, part 1.5: Plated structural elements*. EN 1993-1-5. Eurocode 3, Brussels, Belgium: CEN.

CEN (European Committee for Standardization). 2006b. *Design of steel structures, part 2: Design of steel structures*. Eurocode 3, Brussels, Belgium: CEN.

CEN (European Committee for Standardization). 2007. *Design of steel structures, part 1.12: Additional rules for the extension of EN 1993 up to steel grades S700*. EN 1993-1-12. Eurocode 3. Brussels, Belgium: CEN.

Chen, S.X. 2022. "Local Buckling Behaviour of High Strength Steel and Hybrid I-Sections." Ph.D. dissertation, Dept. of Civil and Environmental Engineering, Hong Kong Polytechnic University.

Chen, S.X., H. Fang, J. Z. Liu, and T.M. Chan. 2022. "Design for local buckling behaviour of welded high strength steel I-sections under bending." *Thin-Walled Struct*. 172: 108792. https://doi.org/10.1016/j.tws.2021.108792

Chen, S.X., J. Z. Liu, and T.M. Chan. 2023a. "Local buckling behaviour of high strength steel and hybrid I-sections under axial compression: Numerical modelling and design." *Thin-Walled Struct.* 191: 111079. https://doi.org/10.1016/j.tws.2023.111079.

Chen, S.X., J. Z. Liu, and T.M. Chan. 2023b. "Material properties and residual stresses of welded high strength steel and hybrid I-sections." *Eng. Struct.* 276: 115293. https://doi.org/10.1016/j.engstruct.2022.115293.

Chen, S.X., J.Z. Liu, and T.M. Chan. 2024. "Design method for cross-section behaviour of hybrid I-girders under uniform bending." *Thin-walled Struct.* 200: 111847. https://doi.org/10.1016/j.tws.2024.111847.

Dassault Systèmes. 2019. *ABAQUS/CAE 2019*. Providence, RI: Dassault Systèmes Simulia Corp.

Fieber, A., L. Gardner and L. Macorini. 2019. "Formulae for determining elastic local buckling half-wavelengths of structural steel cross-sections." *J. Constr. Steel Res*. 159: 493–506. https://doi.org/10.1016/j.jcsr.2019.04.037.

Frost, R.W., and C.G. Schilling. 1964. "Behavior of hybrid beams subjected to static loads." *J. Struct. Div.* 90 (3): 55-88. https://doi.org/10.1061/JSDEAG.0001109.

Gardner, L., A. Fieber, L. Macorini. 2019. "Formulae for calculating elastic local buckling stresses of full structural cross-sections." *Struct.* 17: 2-20. https://doi.org/10.1016/j.istruc.2019.01.012.

Gerard, L., L.Y. Li, M. Kettler, N. Boissonnade. 2019. "Recommendations on the geometrical imperfections definition for the resistance of I-sections." *J. Constr. Steel Res.* 162: 105716. https://doi.org/10.1016/j.jcsr.2019.105716.

Haaijer, G. 1963. "Economy of high strength steel structural members." *Transactions of the American Society of Civil Engineers.* 128 (2): 820-842. https://doi.org/10.1061/TACEAT.0008791.

Joint American Society of Civil Engineers-AASHO Committee on Flexural Members. 1968. "Design of hybrid steel beams." *J. Struct. Div.* 94 (6): 1397-1426. https://doi.org/10.1061/JSDEAG.0001973.

Kamtekar A.G., J.B. Dwight and B.D. Threlfall. 1972. "*Tests on hybrid plate girders (Report 2)*", Report No. CUED/C-Struct/TR Cambridge.

Kamtekar A.G., J.B. Dwight and B.D. Threlfall. 1974. "*Tests on hybrid plate girders (Report 3)*", Report No. CUED/C-Struct/TR41 Cambridge.

Lew, H.S., and A.A. Toprac. 1967. "*Static tests on hybrid plate girders*." Austin: Center for Highway Research, TX: The University of Texas.

Mvola, B., P. Kah, J. Martikainen, and R. Suoranta. 2016. "Dissimilar high-strength steels: fusion welded joints, mismatches, and challenges." *Rev. Adv. Mater. Sci.* 44: 46–159. https://www.ipme.ru/e-journals/RAMS/no_24416/03_24416_mvola.pdf.

512 Shokouhian, M., and Y.J. Shi. 2015. “Flexural strength of hybrid steel I-beams based on slenderness.” *Eng.*
513 *Struct.* 93: 114-128. https://doi.org/10.1016/j.engstruct.2015.03.029.
514 Wang, C. S., L. Duan, Y. F. Chen, and S. C. Wang. 2016. “Flexural behaviour and ductility of hybrid high
515 performance steel I-girders.” *J. Constr. Steel Res.* 125: 1-14. https://doi.org/10.1016/j.jcsr.2016.06.001.
516 White, D.W. 2003. *Improved Flexural Design Provisions for I-Shaped Members and Channels*. Accessed
517 16th March 2021. https://www.aisc.org/globalassets/aisc/manual/15th-ed-ref-list/improved-flexural-design-
518 provisions-for-i-shaped-members-and-channels.pdf.
519 Yun, X. and L. Gardner. 2017. “Stress-strain curves for hot-rolled steels.” *J. Constr. Steel Res.* 133: 36–46.
520 http://dx.doi.org/10.1016/j.jcsr.2017.01.024.
521 Ziemian, R. D. 2010. *Guide to Stability Design Criteria for Metal Structures*, Sixth Edition. John Wiley &
522 Sons, Inc.
523 Zhu, Y.F., X. Yun, and L. Gardner, 2023. “Behaviour and design of high strength steel homogeneous and
524 hybrid welded I-section beams.” *Eng. Struct.* 275: 115275. https://doi.org/10.1016/j.engstruct.2022.115275.
525

Table 1. Summary of hybrid I-beam tests subjected to uniform bending

Reference	Nominal yield strength		f_{yw}/f_{yf}	Number of specimens
	Flange (f_{yf})	Web (f_{yw})		
Frost and Schilling (1964)	690	345	0.5	2
		230	0.33	
Lew and Toprac (1967)	690	250	0.36	5
Kamtekar et al. (1972; 1974)	380	275	0.72	4
Shokouhian and Shi (2015)	460	355	0.77	3
Wang et al. (2016)	420	345	0.82	1
	485		0.71	3
	500		0.69	1

Table 2. Definition of each class for cross-sections subjected to flexure in codes

Required flexural behavior	Design codes					
	AASHTO specification			Eurocode 3		
	Cross-section classification	Slenderness limit		Cross-section classification	Slenderness limit	
		Flange (compression)	Web (bending)		Flange (compression)	Web (bending)
$R_{cap} \geq 3$ and $M_u \geq M_p$	Compact	0.38ε	3.76ε			
				Class 1	0.31ε	2.46ε
$M_u \geq M_p$, but $R_{cap} < 3$	Noncompact	[a] $0.56\sqrt{E/f_{yr}}$	[b] $\left(3.1+\frac{5.0}{\alpha_{wc}}\right)\varepsilon$	Class 2	0.34ε	2.84ε
$M_p > M_u \geq M_y$				Class 3	0.48ε	4.25ε
$M_y > M_u$	Slender	-		Class 4	-	

Note: For the doubly symmetric I-shaped sections, $\varepsilon = \sqrt{E / f_{yf}}$.

[a] f_{yr} is taken as the smaller of $0.7f_{yf}$ and f_{yw}, but not less than $0.5f_{yf}$.

[b] α_{wc} is ratio of two times the web area in compression to the area of the compression flange, but $4.6 \leq \left(3.1+5.0/\alpha_{wc}\right) \leq 5.7$.

Table 3. Average material characteristics of steel plates

Steel plate	E (GPa)	ε_y (%)	ε_{sh} (%)	ε_u (%)	f_y (MPa)	f_u (MPa)
Q690-F	217.4	0.377	3.42	6.75	819.5	848.4
Q690-W	216.1	0.365	2.46	6.86	788.9	834.5
Q460-W	215.8	0.241	1.13	13.6	520.9	663.5
Q355-W	220.0	0.183	1.36	15.6	402.2	563.7

Table 4. Measured section geometrical characteristics of I-section test specimens

Specimen	$b_{f,t}$ (mm)	$b_{f,b}$ (mm)	$t_{f,t}$ (mm)	$t_{f,b}$ (mm)	H (mm)	t_w (mm)	R_h	$\frac{h_w}{t_w}\sqrt{\frac{f_{yf}}{E}}$	Web class	
									AASHTO Specification	Eurocode 3
4P-H310-690W	109.3	111.4	9.52	9.56	305.8	6.23	1.000	2.85	C	2
4P-H310-460W	111.5	111.6	9.62	9.56	308.5	6.00	0.962	2.98	C	3
4P-H310-355W	111.3	109.0	9.58	9.48	307.5	6.68	0.923	2.67	C	2
4P-H350-690W	111.3	109.3	9.56	9.54	348.5	6.33	1.000	3.22	C	3
4P-H350-460W	109.9	109.9	9.56	9.54	347.5	5.96	0.958	3.41	C	3
4P-H350-355W	110.5	109.8	9.58	9.56	348.0	6.63	0.916	3.07	C	3
4P-H440-690W	109.3	109.0	9.53	9.43	438.2	6.25	1.000	4.15	N	3
4P-H440-460W	109.1	111.1	9.54	9.54	438.3	6.12	0.948	4.24	N	4
4P-H440-355W	109.5	111.4	9.54	9.43	438.0	6.52	0.907	4.32	N	4

Table 5. Moment-rotation characteristics of specimens

Specimen	$M_{u,test}$ (kN×m)	M_p (kN×m)	$M_{u,test}/M_p$	R_{cap}	$M_{u,FE}/M_{u,test}$
4P-H310-690W	386.1	356.4	1.08	1.43	0.992
4P-H310-460W	343.3	327.0	1.05	1.47	0.981
4P-H310-355W	333.6	311.7	1.07	2.01	0.981
4P-H350-690W	449.0	428.0	1.05	0.91	0.980
4P-H350-460W	400.5	373.8	1.07	1.54	0.966
4P-H350-355W	397.3	363.8	1.07	1.73	0.963
4P-H440-690W	583.3	582.6	1.00	0.32	0.941
4P-H440-460W	524.6	508.0	1.03	0.72	0.949
4P-H440-355W	507.0	482.4	1.05	0.98	0.966
Max					0.992
Min					0.941
Mean					0.969
CoV					0.017

Table 6. True stress-strain parameters used in simulation analysis

Steel grade	E (GPa)	$f_{y,true}$ (MPa)	$\varepsilon_{y,true}$ (%)	$f_{sh,true}$ (MPa)	$\varepsilon_{sh,true}$ (%)	$f_{u,true}$ (MPa)	$\varepsilon_{u,true}$ (%)
Q690	210	766	0.365	781.2	1.616	875.3	6.14
Q460	210	521	0.248	534.8	2.392	702.6	10.05
Q355	210	403	0.192	407.5	1.165	651.5	14.30

Table 7. Geometric characteristics of representative I-sections

Series	I-Sections	Critical plate	b_f	h_w	$\frac{b_f}{t_f}\sqrt{\frac{f_{yf}}{E}}$	$\frac{h_w}{t_w}\sqrt{\frac{f_{yf}}{E}}$	AASHTO Specification		Eurocode 3		Number of models
							Flange	Web	Flange	Web	
$M_u > M_p$	B40H100	Web	40	100	0.24	1.00	C	C	1	1	3
	B80H100	Flange	80	100	0.48	1.00	C	C	1	1	3
	B80H200	Web	80	200	0.48	2.01	C	C	1	1	3
$M_p>M_u>M_y$	B160H200	Flange	160	200	0.97	2.01	N	C	3	1	3
	B120H400	Web	120	400	0.72	4.03	C	NC	2	3	3
$M_y>M_u$	B220H600	Web	220	600	1.33	6.04	N	S	4	4	3
	B340H600	Flange	340	600	2.05	6.04	S	S	4	4	3
Total amount											21

Table 8. Elastic critical local buckling moment of representative I-sections

Series	I-Sections	Critical plate	Elastic local buckling moment (kN×m)		$M_{cr,Gardner}/M_{cr,FE}$
			$M_{cr,Gardner}$	$M_{cr,FE}$	
$M_u > M_p$	B40H100	Web	896	945	0.95
	B80H100	Flange	670	664	1.01
	B80H200	Web	1008	1023	0.99
$M_p > M_u > M_y$	B160H200	Flange	649	646	1.00
	B120H400	Web	902	932	0.97
$M_y > M_u$	B220H600	Web	1008	1038	0.97
	B340H600	Flange	859	874	0.98

Table 9. Moment-rotation characteristics of representative I-sections

Series	I-Sections	Critical plate	Q690W			Q460W			Q355W		
			M_u/M_p	R_{cap}	M_u/M_y	M_u/M_p	R_{cap}	M_u/M_y	M_u/M_p	R_{cap}	M_u/M_y
$M_u > M_p$	B40H100	Web	1.146	14.4	-	1.137	15.0	-	1.132	15.3	-
	B80H100	Flange	1.087	7.3	-	1.071	7.2	-	1.066	7.1	-
	B80H200	Web	1.020	1.9	-	1.021	2.8	-	1.025	3.6	-
$M_p>M_u>M_y$	B160H200	Flange	0.972	-	1.078	0.987	-	1.057	0.991	-	1.053
	B120H400	Web	0.935	-	1.082	0.971	-	1.041	0.984	-	1.035
$M_y>M_u$	B220H600	Web	-	-	0.834	-	-	0.827	-	-	0.825
	B340H600	Flange	-	-	0.702	-	-	0.677	-	-	0.669

Table 10. Magnitude of local geometrical imperfection for studied I-sections with $M_u > M_p$

I-Sections	Critical plate	Four-point loading			Axial compression		
		$e_{f,max}$ (mm)	$e_{w,max}$ (mm)	$e_{w,max}/e_{f,max}$	$e_{f,max}$ (mm)	$e_{w,max}$ (mm)	$e_{w,max}/e_{f,max}$
B40H100	Web	0.27	0.50	1.85	0.07	0.50	7.14
B80H100	Flange	0.74	0.25	0.34	0.74	3.84	5.19
B80H200	Web	0.70	1.00	1.43	0.17	1.00	5.88